International Journal of Research and Review
[Indexed, Peer-Reviewed Journal]
Volume 12; Issue: 12; December 2025
Website: www.ijrrjournal.com
Research Paper *E-ISSN: 2349-9788; P-ISSN: 2454-2237*

Lithostructural Controls on Orogenic Gold at the Kiesta C Deposit, Sabodala-Massawa District, Senegal

Ibrahima Dia[1], Ibrahima Sow[1]

[1]Polytech Diamniadio, Amadou Mahtar Mbow University, Dakar, Senegal.

Corresponding Author: Ibrahima Dia

DOI: https://doi.org/10.52403/ijrr.20251281

ABSTRACT

Orogenic gold deposits in the Sabodala–Massawa district cluster along crustal-scale shear corridors, but deposit-scale controls on fluid focusing and ore-shoot geometry remain weakly constrained. At the Kiesta C deposit, we test how shear-corridor architecture, jogs and bends, and rheology contrasts at felsic intrusive contacts govern permeability creation, reactivation, and gold distribution. We integrate deposit-scale mapping and pit-wall structural analysis with oriented core logging, petrography, alteration–vein classification, stereographic analysis, and 3D integration of downhole assays. High-grade shoots plunge steeply to the SE, parallel to intersection lineations defined by anastomosing NE–SW shear zones, second-order splays, and intrusive contacts. Gold grades are highest where shear bends and stepovers coincide with albitized quartz–feldspar porphyry and foliated diorite margins, which we interpret to have stiffened and embrittled wall rocks near the brittle–ductile transition, sustaining cyclic crack–seal permeability. A two-stage alteration pattern is recognized: early sericite–carbonate–silica–pyrite halos hosting disseminated Au, overprinted by inner albite–silica–carbonate–tourmaline domains cut by quartz–tourmaline stockworks that host the highest grades. Vein textures and overprinting relationships support repeated brittle failure and sealing of fracture networks during late reactivation of the shear corridor. We propose a conceptual model in which the three-dimensional connectivity of shear corridors, intrusive margins, and brittle fractures—rather than any single "syn-gold" structure—primarily controls ore-shoot continuity and plunge. This framework yields a set of structurally driven, field-based exploration criteria that are applicable within the Sabodala–Massawa district and transferable to analogous orogenic corridors in the Mako Belt.

Keywords: Orogenic gold systems; Mako Belt; shear corridors; albitization; quartz–tourmaline veins; brittle–ductile transition; ore-shoot geometry; Sabodala-Massawa.

1. INTRODUCTION

Orogenic gold systems of the West African Craton (WAC) constitute one of the world's most prolific Paleoproterozoic gold provinces [1], with the Kédougou–Kéniéba Inlier (KKI) hosting numerous deposits aligned along crustal-scale shear systems formed during the Eburnean orogeny [2-9]. Regionally, the Birimian terranes are partitioned into volcanic and sedimentary supergroups and record a multi-stage D1–D3 evolution, in which transpressional strike-slip shearing (D2–D3) reorganized basin architecture and established the

principal pathways for mineralizing fluids [2,3,10-13]. Despite broad agreement on this framework, deposit-scale controls on fluid focusing and ore-shoot geometry remain incompletely resolved at several prospects within the Sabodala–Massawa district.

Within the Sabodala–Massawa district, gold deposits cluster along first and second-order structures kinematically linked to the Main Transcurrent Zone (MTZ) and companion shear systems [14]. These corridors exhibit mixed ductile–brittle behavior, jogs and bends, and repeated reactivation—features widely recognized as favorable for Au deposition [3,5,7,11,15]. However, the relative roles of specific structural elements (bends, stepovers, second-order splays) versus local lithological heterogeneity (e.g., rheology contrasts at intrusive contacts) are still debated. In particular, along the Missira–Kiesta–Nouma corridor, the hierarchy of permeability creation across bends/stepovers, contact zones, and vein arrays is not fully quantified at the deposit scale.

The Kiesta C deposit, located in the western sector of the Missira–Kiesta–Nouma corridor, provides an ideal natural laboratory to address these questions. It juxtaposes high-strain graphitic schists, volcaniclastic hosts, and syn-tectonic felsic to intermediate intrusions within a NE–SW-trending shear corridor. Field and core observations document a progressive deformation sequence from ductile shearing to late brittle faulting, accompanied by multiple alteration stages and vein types. Yet several knowledge gaps remain: (i) the extent to which local rheology contrasts at intrusive margins (e.g., quartz–feldspar porphyry, foliated diorite) modulate the transition from ductile to brittle permeability and thereby control fluid focusing; (ii) the degree to which alteration fronts (sericite–carbonate vs. albite–silica–tourmaline), vein styles (shear-parallel, extensional, stockwork), and gold distribution are spatially and temporally coupled; and (iii) which Kiesta C features represent district-wide Sabodala–Massawa controls versus locally distinctive characteristics relevant for near-mine targeting [3,5,7,11,15].

These uncertainties motivate the central research question of this study: how does the lithostructural architecture at Kiesta C—specifically the interplay of shear corridors, jogs/bends, and rheology contrasts at felsic intrusive contacts—govern the creation, maintenance, and reactivation of permeability pathways that focus auriferous fluids and shape ore-shoot geometry?

To address this question, we pursue three linked objectives:

- Quantify the architecture of strain and permeability by mapping the kinematics and geometry of anastomosing shear corridors, second-order splays, and intersection lineations, and by assessing their relationship to lithological boundaries and intrusive margins.
- Resolve the vein–alteration–deformation sequence by classifying vein sets (shear-parallel quartz±carbonate, extensional veins, quartz–tourmaline stockworks) and alteration envelopes (sericite–silica–carbonate ± pyrite; albite–silica–carbonate–tourmaline), and by establishing their paragenetic relationships to gold.
- Evaluate ore-shoot geometry and its main controls by integrating structural data with assay distributions to test whether high-grade shoots align with intersection lineations and concentrate where rheology contrasts and alteration-induced embrittlement maximize fracture density and connectivity.

Methodologically, we combine deposit-scale mapping and pit-wall structural analysis with detailed core logging, alteration/vein classification, and integration of downhole assays. Stereonet and rose-diagram analyses are used to define mean orientations, dispersion, and intersection trends; grade shells and downhole plots relate gold distribution to vein density and alteration intensity. This multi-scale, integrative approach is designed to capture

both the 3D connectivity of the fracture–vein network and the temporal cyclicity of permeability creation and sealing that characterize orogenic systems in transpressional regimes [3,5,7,11,15].

Our study makes four main contributions. First, we document how bends and stepovers within the NE–SW shear corridor at Kiesta C generate local restraining and releasing segments that focus fluid flow and govern the distribution of ore shoots. Second, we infer that felsic intrusions—particularly quartz–feldspar porphyry bodies and their albitized margins—act as mechanical–chemical catalysts that stiffen and embrittle the wall rock, promoting repeated fracture–sealing cycles along intrusive contacts. Third, we show that gold distribution is tightly coupled to a two-tier alteration system, with sericite–carbonate halos defining broader mineralized corridors and inner albite–silica–carbonate–tourmaline domains hosting the highest grades. Finally, we integrate these structural, lithological, and alteration controls into a deposit-scale framework that builds on previous Sabodala–Massawa studies and can be transferred more broadly to orogenic gold systems where shear-zone architecture and lithology-controlled permeability cycling govern ore-shoot formation.

2. GEOLOGICAL SETTING

2.1. Regional framework

The Sabodala–Massawa district lies within the Kédougou–Kéniéba Inlier (KKI), the westernmost exposure of the Paleoproterozoic Birimian terranes of the West African Craton (WAC) [2,6,8-10,16] (Figure 1). Regionally, the Birimian is organized into NE–SW to ENE–WSW volcanic belts and intervening sedimentary basins and is classically subdivided into two supergroups: the western Mako Supergroup, composed of bimodal volcano–plutonic sequences (ultramafic to mafic volcanic and plutonic suites, including tholeiitic basalts, overlain by calc-alkaline andesitic to felsic units), and the eastern Dialé–Daléma Supergroup, dominated by turbiditic and carbonate metasedimentary rocks; the boundary between them is the crustal-scale Main Transcurrent Zone (MTZ) shear system [2-5,10,13-14,17].

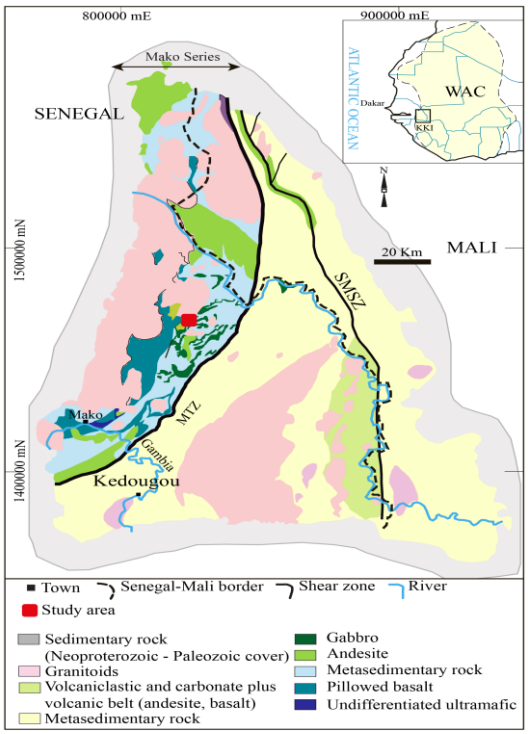

Figure 1. Regional geological context of the Mako Belt (SE Senegal) within the Kédougou–Kéniéba Inlier; showing the study area and major shear zones (SMSZ, MTZ).

Eburnean deformation and magmatism structured the KKI from ca. 2.13 to 2.06 Ga, with three widely recognized deformation stages [4,9,13,17-19]. D1 is a collisional, thrust-dominated phase responsible for crustal thickening and contemporaneous emplacement of large TTG granitoid batholiths; D2 marks a change to a predominantly transpressional regime (sinistral strike-slip shear zones and upright to steep foliations), and D3 records late dextral transcurrent to transtensional overprints [13,14,17]. The D2–D3 shift is pivotal in localizing mineralizing fluids along shear corridors [9]. Eburnean magmatism occurs in suites that include pre-/syn-tectonic batholiths and syn-tectonic TTG massifs dated broadly between ~2213–2060 Ma; these suites encapsulate the transition from early collisional emplacement to later, shear-assisted intrusion during D2–D3 [18,20].

Metamorphism across the WAC Birimian is predominantly greenschist facies with local amphibolite-facies domains (e.g., near certain plutons), reflecting peak conditions during Eburnean crustal thickening and subsequent retrogression during exhumation and shearing. In the regional orogenic gold context, the retrograde path is particularly significant: orogenic Au deposition in West Africa commonly occurred at ~1–4 kbar and 200–450 °C during the greenschist-facies overprint, consistent with widespread observations in Ghana and adjacent belts [1,22]. Altogether, the KKI preserves a polycyclic Eburnean evolution in which early thrusting (D1) and TTG emplacement are followed by transpressive strike-slip shearing (D2–D3) that both reorganized basin architecture and formed the principal fluid pathways for later Au mineralization [3,11-13,17].

2.2. District geology: Missira–Kiesta–Nouma corridor

Within the Sabodala–Massawa mining district, gold deposits cluster along first and second-order structures kinematically linked to the MTZ and companion shear systems [3,7,11]. The district includes several named corridors—Khossanto, Sofia–Sabodala, and Missira–Kiesta–Nouma—whose NE–SW to N–S architecture reflects D2 sinistral transpression overprinted locally by D3 dextral motions [11,14]. In particular, the MTZ separates the Mako and Dialé–Daléma supergroups and focuses Au-bearing fluid flow [14,17]; district-scale structures reactivate during late brittle–ductile to brittle episodes, creating composite vein arrays and dilation sites favorable for gold deposition [3,5,7,11].

In the central Sabodala area, two key structures—the NW-trending “NW Fault” and the subhorizontal to gently dipping “Main Flat”—demonstrate this interplay [3,11,14]. The Main Flat forms a domal, thrust-related architecture within pillow and massive metabasalts and felsic intrusions of the Mako belt; it is associated with pervasive silica–albite–carbonate alteration indicative of relatively open shear environments. The steeper NW Fault shows a more brittle character and sericite–carbonate–quartz alteration, consistent with more channelized fluid flow. Together, these structures capture a multiphase deformation and fluid-flow history in which D2 transpressional shearing set the template for later brittle reactivation and quartz–carbonate–sulfide veining.

The Missira–Kiesta–Nouma corridor occupies the western part of the district (Khossanto–Kiesta trend) and cuts ultramafic and volcanic rocks of the Mako Supergroup [23]. Field and operational mapping consistently show NE–SW-striking to N–S-striking shear bands and second-order splays that partition strain and localize vein systems [11]. This structural array is interpreted as part of the regional D2 sinistral transpressional network, with local late dextral components and brittle reactivation that created mixed shear–extensional vein sets [11,24]. Reactivation along these pre-existing anisotropies is a key control on the distribution of quartz–carbonate veins and ore shoot from Sabodala to Kiesta and Massawa [11].

Intrusive events in the district mirror the regional sequence: early to syn-tectonic TTG granitoids and later granitic to intermediate bodies intruded during D1–D2 to early D3 [20-25]. These intrusions drove contact metamorphism locally (amphibolite facies) and generated rheological contrasts that concentrated strain in adjacent supracrustal rocks. Syn-tectonic emplacement along active shear zones is reflected by elongate pluton geometries and mingling relationships in the Mako belt, reinforcing the coupling of magmatism and deformation during the Eburnean [18,21,23].

2.3. Local geology at Kiesta C

Kiesta C is situated within the Missira–Kiesta–Nouma structural corridor of the Sabodala–Massawa district. The deposit is hosted by volcano-sedimentary sequences ranging from fine to coarse-grained units, intruded by syn-tectonic intermediate to felsic bodies [21]; graphitic schists are locally abundant and intimately tied to deformation, serving as both mechanical anisotropies and chemical traps during fluid flow. At the pit scale, the rock mass records a progression from ductile shearing to brittle deformation, manifest as shear-parallel quartz–carbonate vein sets, extensional veins, and late brittle faults that segment mineralized shoots. Detailed mapping and sections emphasize the role of second-order splays off the regional corridor in focusing alteration and veining, consistent with the broader district behavior (Figure 2).

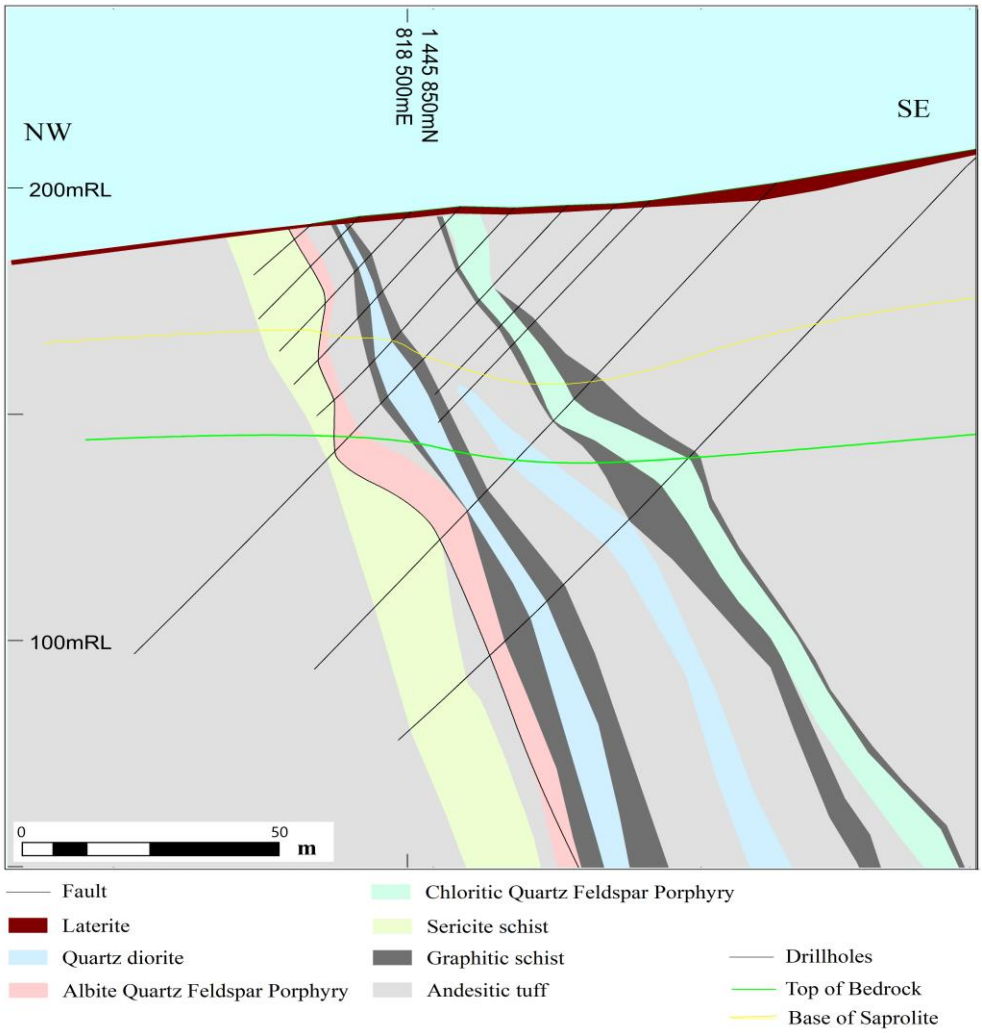

Figure 2. Geological cross-section of the Kiesta C north pit (NW–SE), illustrating lithological units, intrusive contacts and shear zones.

A dioritic intrusive at the western margin of the Kiesta C pit imposes a strong local rheological control. The intrusive's emplacement and pressure effects are inferred to have influenced fracture evolution and fluid pathways; an intense silicification episode—likely post-dating the diorite—produced E–W joints, microfaults, and barren quartz veins in drill core, denoting late, relatively brittle permeability that overprints earlier shear-related mineralization [22,23].

Alteration at Kiesta C comprises multiple stages typical of Eburnean orogenic systems. Early to main-stage sericite–silica–carbonate–pyrite assemblages are overprinted or flanked by albite–silica–carbonate–tourmaline alteration; chloritization and localized tourmalinization occur along structures. These envelopes closely track mineralized shoots and are spatially associated with shear zones and second-order fractures, as shown by pit walls, sections, and kinematic analyses [24].

The local structural grain is consistent with the district-scale pattern: NE–SW to N–S-trending shear planes, with ductile indicators (S–C fabrics, boudinage, shear veins) giving way to crack-seal textures, laminated and brecciated quartz, and late brittle faults. Field photos and structural measurements from Kiesta C illustrate shear-sense indicators (e.g., delta-clasts), buck-type quartz textures, and carbonate-filled extension features—all of which mirror the recognized vein styles and microstructures across the Mako belt (shear, extensional, and stockwork-like veins) [24].

Metamorphic conditions at the deposit reflect the regional pattern of greenschist facies overprinting local amphibolite domains. In this regime, Au mineralization is expected to form during retrogression, with main-stage trapping temperatures of ~240–320 °C and later remobilization at ~120–220 °C recorded elsewhere in the Mako belt; corresponding pressure estimates (~0.75–2.75 kbar) place mineralization at upper to mid-crustal depths (~3–10 km). These pressure–temperature conditions are inferred from fluid-inclusion and microtextural studies on analogous vein systems elsewhere in the Mako belt, rather than directly measured at Kiesta C, but they provide a robust P–T context for the Kiesta C vein-hosted orogenic gold system [22,24].

Previous work throughout the Mako belt establishes a consistent paragenetic sequence that aligns with observations at Kiesta C [23]. Early quartz (buck quartz) and wall-rock silicification are followed by quartz–carbonate–sericite–sulfide stages, with pyrite occurring in two generations and native gold present as inclusions in sulfides and along late microfractures; late chalcedony or carbonate can fill residual vugs. Vein arrays are commonly localized in second and third-order structures adjacent to major shears, reinforcing the role of strain partitioning and episodic pressure drops (hydraulic fracturing) in gold deposition—features that are mirrored by the brecciation, laminated textures, and crack-seal fabrics documented in the Sabodala–Kiesta sector [24].

At the surface, these structural and lithological controls are reflected in a well-defined soil gold anomaly centered on Kiesta C. The main characteristics of this anomaly are summarized in Table 1.

Table 1. Summary of soil gold anomaly at Kiesta C.

Parameter	Value / Description
Anomaly length	~1.9 km
Anomaly width	~100–450 m
Anomaly threshold	>50 ppb Au in soil
Maximum soil values	Up to 500 ppb Au
Host lithologies for strongest anomaly	Altered felsic rocks
Background in graphitic schists	~100 ppb Au

3. MATERIALS & METHODS

3.1. Field mapping and structural data acquisition

Geological mapping was conducted at 1:2,000–1:5,000 scales over the Kiesta C corridor, combining pitwall traverses, scanlines at ~15 m spacing, and targeted station mapping on key structures and lithological contacts. For each station, we recorded lithology, alteration, vein type/texture, vein density, and structural elements (foliation, lineation, shear planes, fold axes, and fracture sets). Orientation data were processed with Dips™ (lower-hemisphere, equal-area projections) to compute mean planes, dispersion, and intersection/lineation trends; vein azimuths were summarized with rose diagrams. Outcrop and pitwall locations were surveyed with a high-precision GNSS receiver and integrated in the mine GIS. In total, the structural dataset comprised 18 foliation measurements, 23 shear-vein measurements, 6 extension-vein measurements, and 14 measurements on major structures. These counts correspond to the subsets used for stereonet and rose-diagram analyses.

3.2. Drill core logging and sampling

The analytical dataset used in this paper focuses on a subset of 12 oriented diamond drillholes (KSDD22-0001 to 0012) totaling ~2,850 m, selected for continuous coverage across the principal shear corridor and intrusive contacts. Six of these holes were fully oriented; alpha–beta measurements were used to restore vein and fabric orientations to geographic space. Core was logged systematically for lithology, alteration (intensity and assemblage), vein type/texture/orientation, and structure, following a standardized coding scheme. Sampling targeted all intervals with visible alteration and/or veining at nominal 1.0 m lengths (shortened at sharp contacts); this yielded the assay dataset described below. Table 2 summarizes the reverse circulation (RC) drilling used for grade control and broader resource modelling at Kiesta C; these RC data were used to constrain the resource model but are not part of the quantitative structural dataset. Additional diamond drillholes (e.g., KSDD22-0024) are used to illustrate significant intercepts and grade variability but are not part of the core structural dataset.

3.3. Petrography and mineral chemistry

A petrographic program was completed on representative lithologies, alteration zones, and ore textures. Standard thin sections were described under transmitted/reflected light to document mineralogy, replacement textures, and vein fill. A subset of polished thin sections from mineralized intervals (shear-parallel veins, quartz–tourmaline stockworks, and albitized wallrock) was examined by SEM-EDS to discriminate sulfide species and accessory phases (e.g., tourmaline, carbonates). Thin sections were prepared offsite at an accredited external laboratory immediately after fieldwork to address local preparation constraints.

3.4. Geochemical analyses and QA/QC

Samples were crushed and pulverized to industry specifications at accredited commercial laboratories (ALS Kédougou and the Sabodala mine analytical facilities). Gold was determined by 50 g fire assay with AAS finish (SGS/ALS method FAA505; LOD ~0.01 ppm). Selected intervals were analyzed for a multi-element suite (e.g., As, Sb, Bi, Te, S, Cu, Pb, Zn) by ICP-MS to evaluate pathfinder behavior and alteration halos. The QA/QC program included field or pulp duplicates every 15 samples, certified reference materials inserted at the 20th position of each sequence block, and analytical blanks at the 21st position. QA/QC checks indicated acceptable accuracy and precision (CRMs within tolerance, duplicates with satisfactory repeatability, and blanks typically at or below detection); any failures triggered reassay, and only validated results were retained for interpretation and modeling. Key drilling, sampling, and QA/QC procedures are summarized in Table 2.

Table 2. Summary of drilling, sampling and QA/QC procedures at Kiesta C.

Item	Description
Grade control drilling grid	10 m × 10 m within the Kiesta C pit
Drillhole orientation	RC holes drilled with an azimuth of N300 and a dip of −50°
RC sample length	1 m downhole
RC sample collection	Cuttings collected in ~50 kg plastic bags, homogenized and split
Analytical sample mass	2.5–3 kg per sample sent to the laboratory
Analytical method (pit wall samples)	Fire Assay with AAS finish (FAA505)
QA/QC – field duplicates	One duplicates every 15 routine samples
QA/QC – standards (CRM)	One certified reference material inserted every 20th sample
QA/QC – blanks	One blank inserted every 21st sample
QC objective	To monitor precision, accuracy and contamination prior to data use in interpretation and modelling

Note: Table 2 reports the RC drilling used for grade control and resource modelling; the structural dataset discussed in this paper is based on oriented diamond drillholes (KSDD-series).

3.5. Data integration and modeling

All field, core, and assay data were compiled in the site GIS and 3D modelling environment. Lithological contacts, intrusive margins, shear zones, vein corridors, and alteration envelopes mapped at surface and in core were digitized and projected into 3D. Grade shells were constructed in Vulcan™ using explicit contacts, structural surfaces, and logged alteration intensities to constrain mineralized volumes and to avoid purely grade-driven envelopes.

Structural datasets used in stereographic and rose-diagram analysis, together with their specific roles in the interpretation, are summarized in Table 3 and Figure 6. Foliation, shear-vein, extension-vein, and vein-corridor orientations were used to define principal strain axes and intersection lineations, and to link ore-shoot geometry to the three-dimensional arrangement of shear planes, lithological contacts, and intrusive margins.

Table 3. Summary of structural measurements used in stereonet and rose-diagram analyses.

Structural element	Number of measurements	Use in the paper
Foliations (S1/S2/S3)	18	Computation of mean foliation plane and lineation trends
Shear veins (quartz–carbonate)	23	Stereonet analysis of shear-controlled vein sets
Extension veins	6	Rose-diagram summary of extensional vein orientations
Major structures (faults/shears)	14	Deposit-scale structural framework and intersection lineations

3.6. Methodological limitations

Several constraints should be noted. (i) A portion of the pit walls comprises blasted faces, which locally obscure small-scale structures and vein textures. (ii) Structural measurements on core are unevenly distributed, with some azimuths and lithologies better represented than others and some holes only partially oriented. (iii) The number of measurements remains modest for certain families (notably extension veins and minor faults), so the corresponding stereonet clusters should be regarded as indicative trends rather than exhaustive populations. (iv) No new geochronological data were generated as part of this study; timing relationships are therefore inferred from structural overprinting relationships and regional analogues. Together, these factors mean that our structural and paragenetic interpretations represent a best-fit framework constrained by the available data rather than a fully quantified model. Future work should therefore prioritize additional oriented drilling, denser structural sampling

of minor vein sets, and geochronological constraints on key vein generations to test and refine this framework quantitatively.

Methodological rationale. Stereographic analysis (lower-hemisphere, equal-area stereonets and rose diagrams) was selected to quantify mean orientations, dispersion, and intersection/lineation trends of fabrics and vein sets, which are essential to evaluate the first-order objective: whether ore-shoot geometry and plunge track the 3-D intersections of shear planes, foliation, and vein corridors. A standardized vein classification (shear vs. extensional vs. quartz–tourmaline stockworks; laminated/crack-seal vs. breccia textures) was adopted to formalize textural and mineralogical criteria underpinning the paragenetic sequence, thereby linking permeability cycling and wallrock reactivity to gold distribution. Together, these methods provide (i) reproducible orientation statistics to test shoot alignment with structural intersections and lineations, and (ii) a consistent descriptive framework to compare alteration–vein stages against downhole assays at deposit scale.

4. RESULTS

4.1. Lithology and intrusive relationships

The Kiesta C area exposes a volcano-sedimentary package intruded by felsic to intermediate bodies [23]. The principal mapped units are: (i) graphitic metasedimentary schists with mylonitic fabrics; (ii) volcaniclastic tuffs variably sericitized; (iii) foliated diorite; and (iv) quartz–feldspar porphyry (QFP). The QFP is competent and occurs as meter to decametre-scale bodies and dykes, locally forming porphyritic stocks [23]. Contacts between QFP and country rocks are sharp to gradational at the outcrop scale; chilled margins were not observed. Diorite is foliated parallel to the regional fabric and locally encloses xenoliths of the volcano-sedimentary host [23]. The volcano-sedimentary sequence shows a strong penetrative foliation and spaced cleavage. Lithological contacts are commonly parallel to the NE-striking structural grain and are locally transposed within the shear corridor [23] (Figure 3).

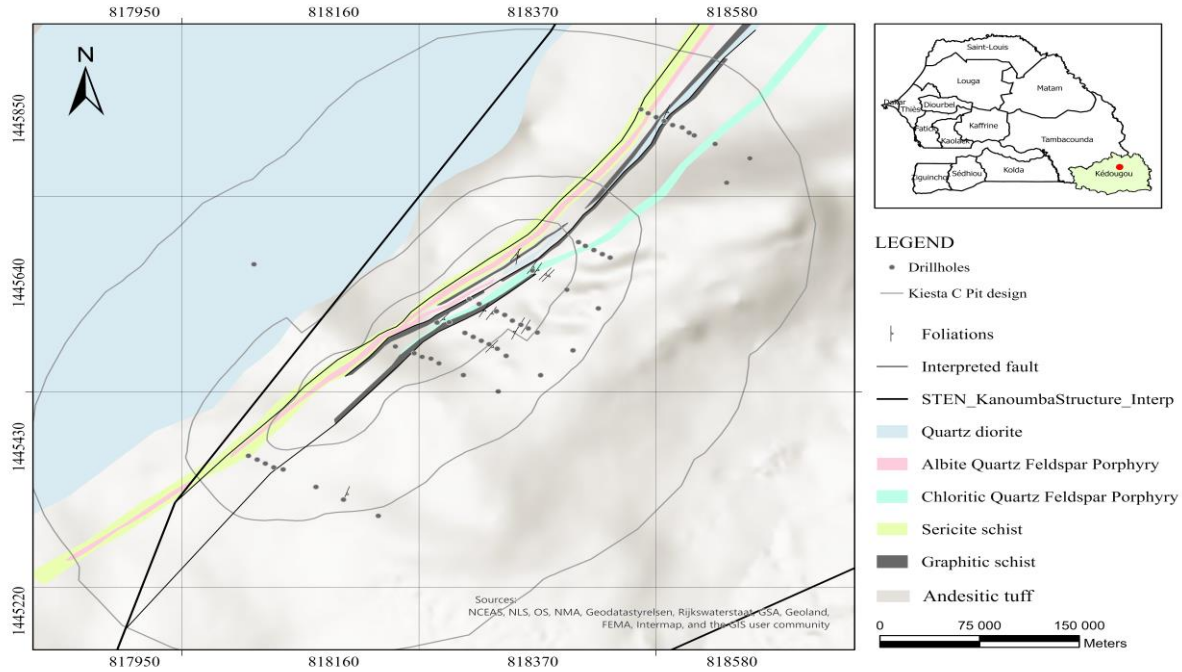

Figure 3. Lithostructural map of the Kiesta C deposit at 200 m RL, showing lithologies, shear zones, vein corridors, and sample locations.

4.2. Alteration assemblages and intensity (sericite–carbonate, albite–silica–tourmaline, chlorite, graphite, sulfides)

Hydrothermal alteration at Kiesta C organizes into two spatially overlapping, compositionally distinct envelopes that parallel the principal shear zone.

- A first, broad envelope (~50 m wide along the principal shear corridor) is defined by pervasive sericite–silica–carbonate ± pyrite replacement of the host rocks. Sericitization affects feldspars; carbonates occur as ankerite ± calcite disseminations and vein selvages; pyrite is disseminated and as thin veinlets. Intensity increases toward zones of highest strain, where alteration becomes diffuse but continuous along foliation planes (Figure 4).

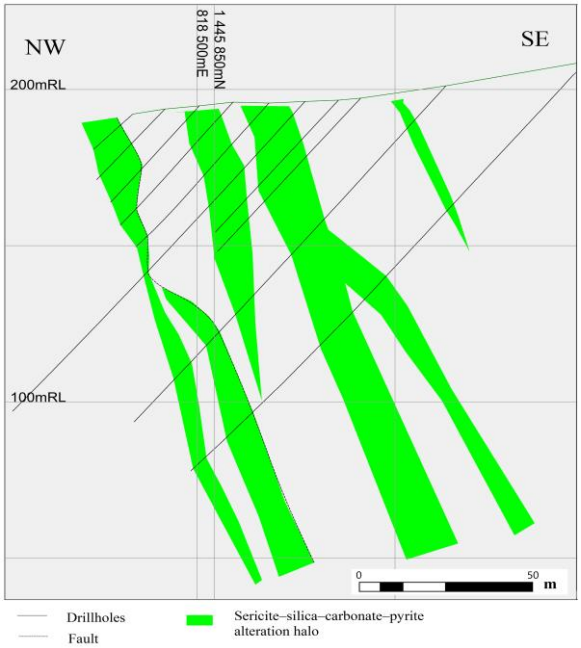

Figure 4. Cross-section of the outer alteration envelope: sericite–silica–carbonate ± pyrite alteration halo along the principal shear corridor.

A second, internal envelope is characterized by albite–silica–carbonate–tourmaline. It is spatially nested within the first and overprints QFP, foliated diorite, and portions of the wall rock. Albitization is pervasive to patchy within QFP and along fracture halos; tourmaline occurs as vein infill and disseminations near veins and fracture networks. Silicification manifests both as pervasive bleaching and as quartz vein stockworks; local hydrothermal breccias are present (Figure 5).

These two alteration envelopes can be grouped into two main hydrothermal stages that differ in deformation regime, mineral assemblage and gold tenor. Their key features are summarized in Table 4.

Table 4. Summary of hydrothermal alteration stages and their relation to gold mineralization at Kiesta C.

Stage	Deformation regime	Main mineral assemblage	Fluid characteristics / T (°C) [1]	Typical gold grade style
1	Ductile	Sericite–carbonate–silica–pyrite	Hot fluids (200–400 °C) enriched in Fe, Au, K, SiO_2, H_2S, Ca, CO_2	Low to moderate-grade Au, disseminated sulfides in sericite-altered zones
2	Ductile–brittle	Silica–albite–carbonate–tourmaline	Fluids rich in silica, Na, Au, B, etc.	Higher-grade Au in albitized QFP with quartz–tourmaline veinlets and at intrusive contacts

[1] **Typical ranges from analogous orogenic systems.**

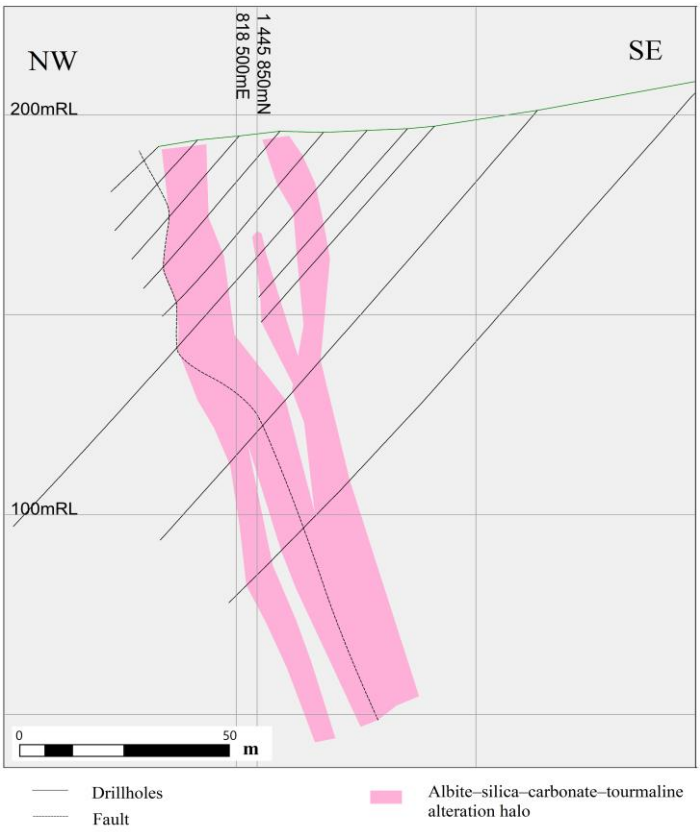

Figure 5. Cross-section of the inner alteration envelope: albite–silica–carbonate–tourmaline alteration and associated quartz–tourmaline stockworks.

Chloritization is observed in sheared volcaniclastic rocks and along discrete slip surfaces. Graphite is abundant in the mylonitic metasediments, defining dark schists within the shear zone. Sulfides are dominated by pyrite as disseminations, veinlets, and coatings on shear planes.

4.3. Vein types and textures (Qz±Cbt, Qtz–Tour, breccias; orientation, density)

Field mapping and core logging identify three principal vein sets, distinguished by orientation, texture, and mineralogy, as summarized below:

- Shear veins: quartz ± carbonate ± sulfide, NE-striking with steep SE dips, parallel to the main foliation within the ductile shear corridor. Veins are laminated to foliated and locally folded; sulfides line slip surfaces.
- Extension veins: quartz ± carbonate, subhorizontal to gently dipping, cutting the foliation at high angle. Veins are millimetre to centimetre-scale and occur as arrays.
- Quartz–tourmaline veins and stockworks: abundant within albitized QFP and adjacent diorite and wall rocks; tourmaline fills vein cores and selvages. Local hydrothermal breccias display angular clasts cemented by quartz.

Vein density is highest inside albitized QFP and along the principal shear bands; late, thick E–W quartz veins occur across the open pit and are largely barren.

4.4. Deformation features (S–C fabrics, shear bands, folds, brittle reactivation; D1–D3 sequence)

The structural grain is NE–SW. The principal foliation strikes around N040 and dips steeply to the SE. A stretching lineation plunges steeply SE (~N130° trend). Within the corridor, rocks display S–C fabrics, shear bands, and mylonitic textures; graphite-rich schists mark the highest strain zones. Chevron folds with subhorizontal axial planes occur in the wall rocks; microfolds have axial planes subparallel to foliation. Shear-parallel quartz veins are

commonly boudinaged and locally folded. Late brittle features include joints, microfaults, and an E–W to NW–SE fracture set cutting earlier veins; a prominent E–W quartz vein crosses the pit (Figure 6).

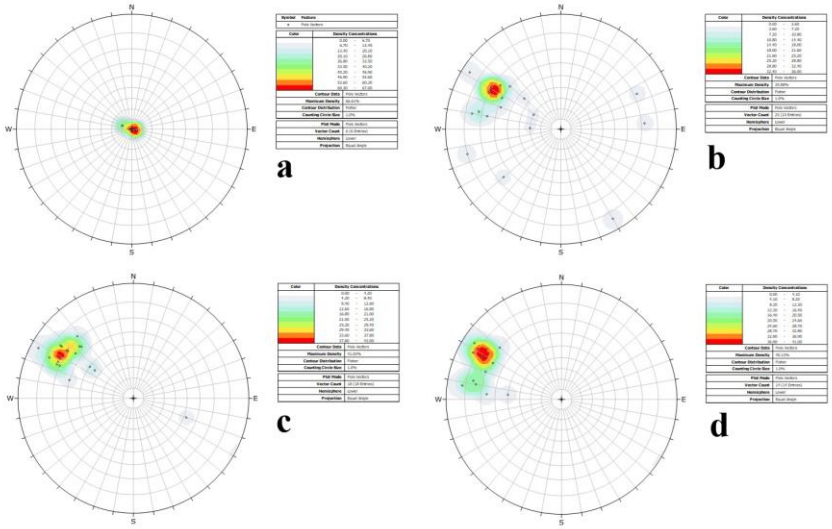

Figure 6. Structural analysis at Kiesta C: stereonets of (a) extension veins; (b) shear veins; (c) foliation; and (d) major faults. The combined orientations define a steep SE-plunging intersection lineation (arrow) that is parallel to the plunge of the main ore shoots, highlighting the key geometric link between 3D structural connectivity and ore-shoot geometry.

4.5. Mineralization styles and paragenesis (sulfide assemblages, timing vs. deformation/veining)

Gold distribution at Kiesta C is restricted to two main mineralization styles, which are outlined here, together with the associated paragenetic progression.

- Disseminated and shear-plane-hosted sulfides within the sericite–silica–carbonate ± pyrite envelope, spatially coincident with zones of highest ductile strain. Pyrite occurs as disseminations, thin veinlets, and coatings along S–C surfaces and shear veins.
- Higher-grade mineralization within the albite–silica–carbonate–tourmaline domain, particularly in albitized QFP cut by quartz–tourmaline stockworks. Sulfides occur with quartz–tourmaline vein fill and in adjacent altered halos.

Selective chip sampling along the north pit wall provides a quantitative illustration of grades and geological controls within these mineralized domains. Summary statistics for this sampling campaign are given in Table 5.

Table 5. Summary statistics of selective chip samples collected on the north pit wall at Kiesta C.

Parameter	Value / Description
Number of samples	17
Sampling context	Selective sampling along a ~50 m long wall (175–172.5 RL)
Analytical method	Fire Assay with AAS finish (FAA505)
Grade range	0.03–4.74 g/t Au
Mean grade	0.61 g/t Au
Cut-off grade used for this wall	0.6 g/t Au
Number of samples above cut-off	3 samples (no. 5, 7 and 17)
Grades of samples above cut-off	1.17, 1.61 and 4.74 g/t Au
Width of slightly mineralized domain	~2 m
Geological control on this domain	Strong ductile deformation, intensely deformed albite-altered QFP in contact with a N–S ductile fault

A paragenetic sequence reconstructed from core and outcrop observations distinguishes an early, ductile mineralization stage from later brittle reactivation. The early stage comprises foliation development with sericitization and disseminated pyrite, followed by quartz–carbonate shear veins with sulfide coatings. A subsequent stage is marked by quartz–tourmaline veining and stockworks coincident with pervasive albitization, which locally overprint the earlier sericite–carbonate assemblages. The latest, predominantly brittle stage is expressed by mostly barren E–W quartz veins and reactivation of earlier structures. This progression underpins the distinction between early, broadly distributed mineralization and later, more focused high-grade shoots, as reflected in the integrated sections and the conceptual model (Figure 10).

4.6. Geochemical/assay patterns (Au distribution, pathfinders, metal ratios)

Downhole assays define continuous mineralized intervals within the core of the deposit (Figure 7). A representative intersection in KSDD22-0005 records 23 m @ 4.23 g/t Au from 173–196 m. Local high-grade samples exceed 14 g/t Au over short lengths. In the northern sector (e.g., KSDD22-0008), mineralization is present but with shorter runs and lower average grades (e.g., 7 m @ 1.23 g/t Au from 129–136 m). Grade shells align with the NE structural grain and concentrate where vein density is highest and alteration intensity is strongest (Figure 8).

Representative significant intercepts from the Kiesta C diamond drilling program are listed in Table 6 to illustrate the range of mineralized intervals and their spatial distribution within the deposit.

Table 6. Selected significant gold intercepts from Kiesta C diamond drilling.

Hole ID	From (m)	To (m)	Interval (m)	Avg. Au (g/t)	Comment / Position
KSDD22-0005	173	196	23	4.23	Central part of the ore body
KSDD22-0008	129	136	7	1.23	Northern sector, lower grades
KSDD22-0003	142	148	6	2.75	Intermediate-grade intercept
KSDD22-0024	182	185	3	14.27	Short, very high-grade intercept

Beyond individual intercepts, core logging and wall-mapping highlight consistent relationships between gold grade, vein density and alteration assemblages. Intervals with sparse veining typically carry low to moderate Au values, whereas domains where several generations of quartz–carbonate and quartz–tourmaline veins overlap host the most continuous runs of elevated grades. The longest and highest-grade intersections listed in Table 6 come from the central stockwork zone, where fracture density and veining are at their maximum.

At the scale of alteration halos, gold is preferentially concentrated within the albite–silica–carbonate–tourmaline domain, while the broader sericite–carbonate ± pyrite envelope defines a lower-grade, more diffuse halo around the main orebody. Multi-element analyses (e.g., As, Sb, Bi, Te) on selected intervals show enrichments that closely track the Au anomalies and the sericite–carbonate to albite–silica–tourmaline alteration transitions. In particular, As and Sb display strong positive associations with Au, consistent with typical orogenic gold pathfinder patterns and reinforcing the structural and alteration controls inferred from Au alone. The north-pit chip-sampling results (Table 5) and the integrated sections in Figures 7 and 8 both show that the highest grades are systematically associated with strongly albitized quartz–feldspar porphyry and adjacent quartz–tourmaline stockworks, whereas late, thick E–W quartz veins cutting the system are largely barren.

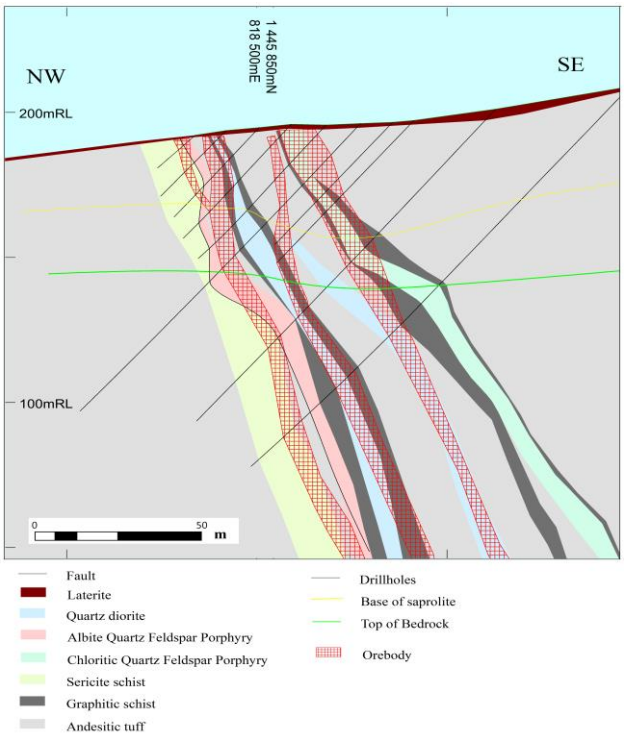

Figure 7. Integrated geological section (RC + DD) showing lithology and mineralized domains.

Within mineralized envelopes, Au correlates with pyrite abundance at the hand-sample and thin-vein scale; late E–W quartz veins are generally barren.

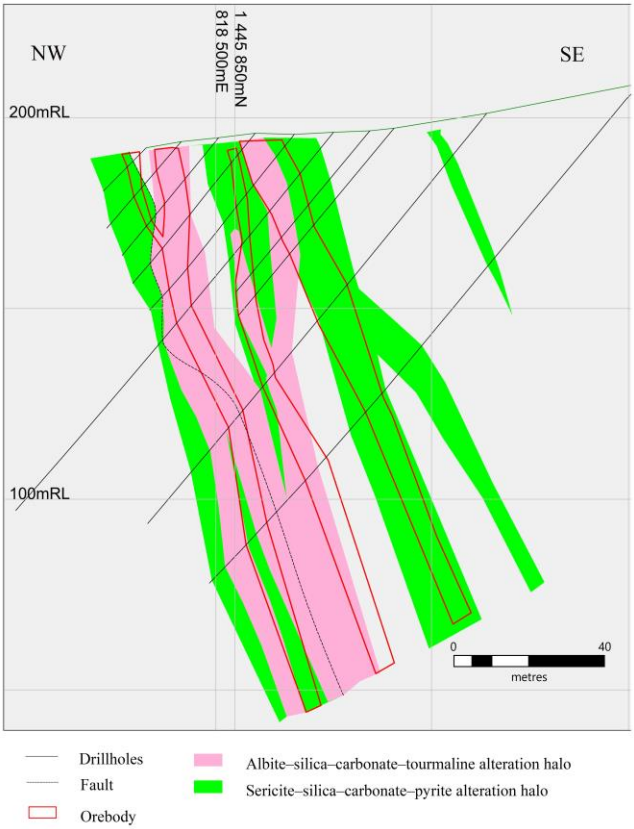

Figure 8. Downhole assay patterns and grade shells: Au distribution relative to alteration zones and vein density.

4.7. Geometry of ore shoots (plunge/orientation, relation to intersections, competency contrasts)

At deposit scale, mineralized zones are elongated NE–SW parallel to the principal foliation, with grade continuity following the structural corridor. Ore shoots exhibit a steep SE plunge consistent with the observed stretching lineation. Higher-grade shoots coincide with (i) intersections between shear-parallel veins and cross-fracture arrays, and (ii) competent lithologies, especially albitized QFP, where fracture density and stockwork development are greatest. The mineralized envelope narrows across graphite-rich mylonites and widens within competent intrusive domains; late E–W fractures locally offset or terminate mineralized veins without introducing additional gold. In the integrated geological section (Figure 7), high-grade shells are systematically aligned along steep SE-plunging axes that parallel the intersection lineations between NE-striking shear veins and N–S to NNE–SSW structures. Figures 8 and 10 further illustrate how these ore-shoot axes are localized where intersection lineations coincide with the transition from sericite–carbonate halos into albite–silica–carbonate–tourmaline domains along intrusive contacts.

5. DISCUSSION

5.1. Lithostructural Architecture and Fluid Focusing

The distribution of gold at Kiesta C is best understood in terms of a multi-scale litho-structural architecture in which a NE–SW-trending, transpressional shear corridor is partitioned into anastomosing high-strain zones separated by relatively competent lithological panels (Figure 9). This picture is consistent with regional models in which transpressional shear zones and second-order structures organize strain and fluid flow within the Kédougou–Kéniéba Inlier and the wider Sabodala–Massawa district [1,3,11,28–30,34]. At Kiesta C, the principal shear zone is accompanied by subsidiary shear strands, local bends and jogs, and steeply plunging intersection lineations, which together define the three-dimensional framework within which ore shoots develop.

Our structural and assay data indicate that gold grades are systematically enhanced where several favorable features coincide: (i) the intersection of NE–SW shear corridors with oblique to transverse structures, (ii) abrupt changes in shear-zone orientation (bends, jogs and stepovers) that promote local dilation or mixed strike-slip–reverse kinematics, and (iii) contacts between mechanically contrasting lithologies, especially between mafic volcanic–volcaniclastic rocks and felsic intrusive bodies. In these locations, shear strain is partitioned into narrow, high-strain panels and damage zones, and the resulting network of shear planes, extensional fractures and sheared vein arrays creates an efficient permeability skeleton for auriferous fluid focusing. High-grade ore shoots plunge steeply to the SE, broadly parallel to the measured intersection lineations, supporting the interpretation that shoot geometry is controlled by the three-dimensional stacking of structural and lithological heterogeneities rather than by a single “ore-controlling” fault surface. Additional 3D modelling of the fracture–vein network would be needed to quantify this relationship beyond the current dataset [27].

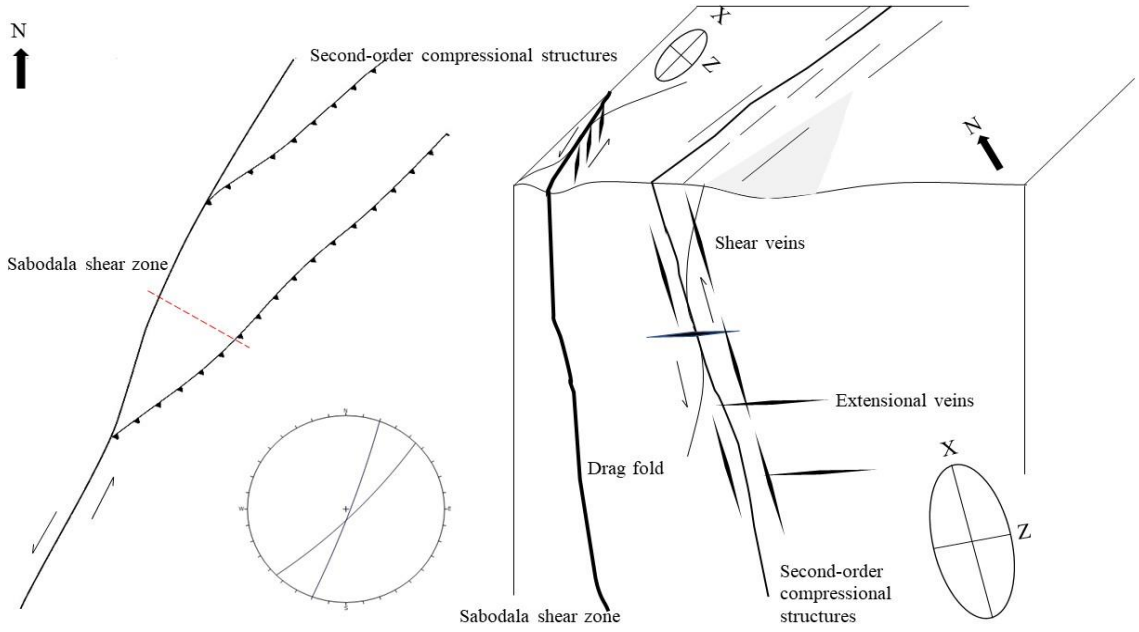

Figure 9. Deposit-scale structural framework: anastomosing shear corridors, bends, stepovers, and associated damage zones (schematic block diagram).

Where shear planes interact with lithological contacts or preexisting anisotropies (e.g., primary bedding, early metamorphic fabrics), permeability anisotropy is amplified, creating channelized pathways [26-27]. Rheology contrasts play a critical role: fine-grained, carbonaceous or iron-rich metasediments deform viscously and localize strain, while more competent intrusive or volcaniclastic units fracture and maintain open space during transient drops in effective stress [26,28]. Field observations show that rheology contrasts correlate with increased fracture density in competent units (e.g., QFP) versus ductile strain localization in graphitic schists. This suggests coupled ductile-brittle behavior, though direct mechanical measurements would be needed to confirm the deformation mechanisms [28].

At the district scale, similar structural templates characterize Sabodala Main and related ore bodies, where composite vein arrays and dilation zones formed during late brittle–ductile to brittle reactivation of crustal-scale shears (e.g., the "Main Flat" and "NW Fault") [3,29,31]. The Kiesta C pattern—ore concentration at bends and structural intersections—thus accords with established Sabodala–Massawa controls, while emphasizing the importance of local architecture in sustaining fluid flux through time. These features are consistent with widely documented processes in orogenic systems, in which restraining/releasing geometries, damage-zone development, and connectivity across shear splays govern fluid focusing and ore-shoot continuity [1,7,35,36].

5.2. Mechanical–Chemical Roles of Felsic Intrusions

Felsic intrusions at Kiesta C—particularly quartz–feldspar porphyry (QFP) and foliated diorite—play a pivotal mechanical role in controlling permeability and gold distribution. These bodies are preferentially emplaced along, or immediately adjacent to, the main shear corridor and are subsequently overprinted by deformation. Relative to the surrounding mafic volcano-sedimentary rocks, QFP behaves as a mechanically distinct lens that initially concentrates strain along its margins; once pervasively fractured and veined, it becomes prone to localized brittle failure and damage-zone development. We infer that this evolution from competent intrusive cores to embrittled, vein-rich margins is

central to the localization of dense vein networks and high-grade mineralization along intrusive contacts [7,9,22,28].

Chemically, alkali metasomatism (notably albitization) modifies the rheological properties of intrusive margins by increasing feldspar and silica content and by introducing tourmaline and sulfides. These changes likely stiffen the wall rocks and enhance their propensity for brittle fracturing during stress cycling, thereby reinforcing mechanically controlled damage zones along intrusive contacts. The systematic association of the highest gold grades with albitized QFP margins, quartz–tourmaline stockworks and crack–seal veins is consistent with models in which chemical hardening of intrusive margins localizes damage-zone development and repeated fluid focusing [25,26,29,31–33].

Across the Sabodala–Massawa district, intrusive–shear interactions are a recurrent motif; technical summaries similarly highlight silica–albite–carbonate alteration around shear-parallel structures and intrusive contacts as markers of relatively open shear environments. Kiesta C fits this motif but further underscores the persistence of permeability cycling at intrusive margins [26-27]. The broader orogenic literature recognizes comparable intrusive-proximal stiffening and fracture connectivity in Archean and Paleoproterozoic camps where porphyry dykes and felsic plugs act as "hard" inclusions and permeability anchors during transpression [27-28]. The multiple vein generations observed along intrusive margins at Kiesta C could reflect hydraulic reactivation over several fluid events [30-31]. However, the timing and number of distinct fluid pulses cannot be firmly established without geochronological constraints on vein formation [7,22,30].

5.3. Vein–Alteration–Deformation Coupling and Cyclicity

Textural relationships at Kiesta C indicate a progressive shift from ductile to brittle-dominated deformation that is tightly coupled to a two-stage alteration–vein sequence. An early sericite–carbonate–silica–pyrite assemblage is associated with ductile to brittle-ductile shearing, shear-parallel quartz±carbonate veins and disseminated sulfides along foliations, generating broad halos of anomalous gold within graphitic schists and related lithologies. A second, more focused stage involves albite–silica–carbonate–tourmaline alteration associated with quartz–tourmaline veins and stockworks that commonly overprint or crosscut the earlier assemblage. In these inner zones, gold grades are significantly higher, and veining is dominated by extensional and hybrid fracture sets that exploit preexisting fabrics and intrusive margins [7,22,30,31].

The observed vein textures—including laminated quartz, crack–seal banding and inclusion trails—together with overprinting relationships between vein sets, support repeated brittle failure and sealing of fracture networks during late reactivation of the shear corridor. These features are compatible with fault-valve behaviour near the brittle–ductile transition, in which overpressured fluids accumulate below the BDT and are episodically released during slip events, leading to cycles of permeability creation and sealing [3,11,14,16,25,26,29,31]. Although the exact pressure–temperature conditions and number of distinct fluid pulses cannot be resolved from the present dataset, the textural evidence and alteration zoning are consistent with progressive upward migration of deformation and fluid flow from more ductile to more brittle structural levels, with the main gold-bearing quartz–tourmaline veining occurring near or just above the BDT [30,36].

5.4. Comparison, regional context, and transferability

At the district scale, Kiesta C shares several hallmarks with other Sabodala–Massawa deposits: localization along crustal-scale shear corridors, ore clustering near major fault intersections, and repeated brittle–ductile reactivation of long-lived structures

[3,11,14,16,29,31]. These features fit well within established orogenic gold models, in which transpressional shear zones and second-order splays act as principal fluid pathways and sites of ore-shoot development [1,3,11,28–30].

The distinctive aspects at Kiesta C concern the relative importance of intrusive-margin rheology contrasts compared with purely structural intersection controls. High-grade shoots are most strongly developed where NE–SW shear bends and stepovers coincide with albitized felsic intrusive margins, producing zones of enhanced fracture density and vein connectivity near the brittle–ductile transition [29,31–33]. In this sense, Kiesta C emphasizes how mechanical and chemical hardening of intrusive margins can localize damage zones and sustain permeability cycling over multiple deformation episodes.

More broadly across West Africa, reviews highlight the recurrent association of orogenic gold with transcrustal shear corridors, long-lived deformation, and episodic brittle reactivation that upgrades earlier mineralization [1,3,11,28–30,34]. Kiesta C fits this pattern but shows that, within a given corridor, intrusive–shear interactions can be as important as first-order fault intersections in controlling shoot geometry. Intrusive–proximal effects at Kiesta C are best viewed as mechanical–chemical catalysts within metamorphic, aqueous–carbonic fluid pathways, rather than as evidence for a necessary magmatic–hydrothermal fluid source [27,29].

The novelty of the Kiesta C study lies in explicitly linking deposit-scale bends and stepovers, intrusive-margin rheology contrasts, and two-tier alteration zonation to ore-shoot geometry within a single, integrated dataset. This formalizes a field-deployable, structurally driven targeting framework that complements existing Sabodala–Massawa models and can be scaled to other orogenic corridors without requiring new geochronology or extensive 3D geophysical surveys [28–30,33,34].

5.5. Implications for Exploration and Near-Mine Targeting

Building on the documented structural, alteration, and veining patterns, the Kiesta C dataset supports the following scale-integrated exploration criteria, translating deposit-scale controls into mappable and testable targets.

- Shear bends and stepovers: Prioritize restraining/releasing segments within master shear corridors where damage zones and breccia pockets are likely.
- Intersection lineations: Map and model the 3D intersections of shear planes, foliations, and vein sets; shoot plunges are expected to align with these lineations.
- Rheology contrasts: Focus on intrusive margins and contacts between stiff and weak units; look for alteration-driven embrittlement (silica/alkali enrichment) that sustains reactivation.
- Alteration footprints: Use sericite–carbonate halos as first-pass footprints and track transitions to silica-rich and sulfide-bearing assemblages toward ore.
- Permeability tiers near the BDT: Depth targeting should consider structural domains where brittle-ductile behavior is inferred, though identifying these horizons precisely remains challenging without 3D seismic data or detailed pressure-temperature constraints from fluid inclusions.
- Reactivated structures: Late brittle faults that segment earlier veins can localize remobilized high grade; geophysical contrasts and vein offset patterns are useful guides [3,11,29].

These recommendations are consistent with best-practice orogenic gold exploration frameworks that stress multiscale architecture, pathway–trap juxtaposition, and cyclic permeability maintenance [1].

5.5. Conceptual Model

We propose a deposit-scale model in which gold mineralization results from the iterative coupling of deformation, permeability

creation, and wall-rock reactivity (Figure 10):

- Architecture: Regional transpression organizes strain into anastomosing shear corridors (Figure 3). Local bends and stepovers, mapped at Kiesta C and illustrated schematically in Figure 9, generate pressure shadows and damage zones that coincide with the principal ore shoots.
- Permeability creation: Competency contrasts at intrusive margins and within rheologically layered sequences foster mixed brittle–ductile behaviour, producing fracture corridors and microporosity, as recorded by dense quartz–carbonate and quartz–tourmaline stockworks along albitized QFP margins (Figures 5, 7–8; Tables 4–6).
- Fluid focusing and reaction: Orogenic fluids ascend along these corridors and concentrate in dilational sites at shear bends and intrusive contacts. Sulfidation of Fe-bearing wall rocks within the sericite–carbonate envelope and subsequent overprinting by albite–silica–tourmaline assemblages precipitate Au with arsenopyrite–pyrite ± base-metal sulfides, consistent with the observed coupling between alteration fronts, sulfide abundance and gold grades (Tables 4–6).
- Cyclicity: The observed crack–seal textures indicate repeated fracture opening and sealing. We infer that such cyclic flow progressively upgraded ore shoots through multiple fluid events, even though the number and absolute timing of these cycles remain unconstrained with the current dataset.
- Shoot geometry: High-grade shoots align with the steep SE-plunging intersection lineation and cluster where (i) shear bends coincide with intrusive contacts, and (ii) alteration has embrittled the host, allowing repeated vein opening, as shown by the 3D grade shells and drill sections in Figures 7–8.

Early sericite–carbonate sulfidation associated with ductile shearing creates the initial chemical trap, while subsequent brittle reactivation and Qtz–Tour stockwork development in albitized domains progressively upgrade grade and extend ore continuity along steep SE-plunging lineations. Late E–W fractures and veins truncate or offset mineralized packages but are largely barren, marking the waning stages of the system.

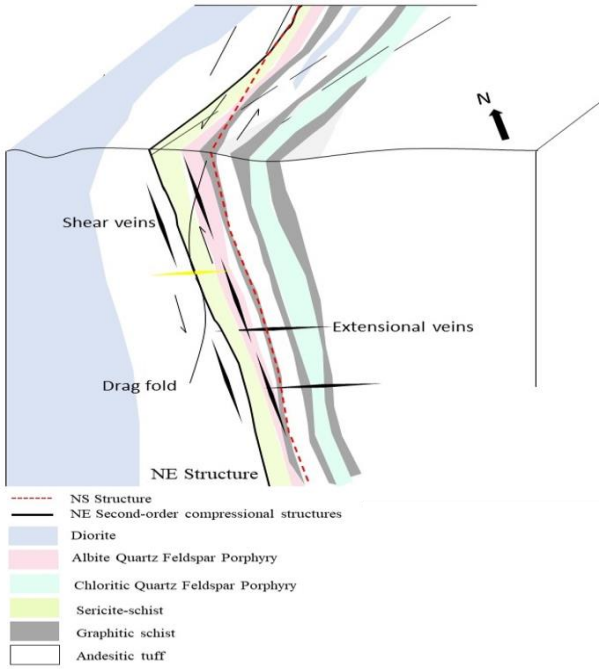

Figure 10. Conceptual four-stage model of gold mineralization at Kiesta C, illustrating deformation–permeability coupling and vein evolution.

6. CONCLUSION

The Kiesta C deposit exemplifies an orogenic gold system developed within an anastomosing NE–SW transpressional corridor where strain, permeability, and gold distribution are jointly controlled by the interplay of shear bends and stepovers, lithological contacts, and intrusive margins. Two nested alteration envelopes—a broad sericite–carbonate halo and an inner albite–silica–carbonate–tourmaline domain—focus mineralization along segments where the structural and rheological architecture is most favorable.

Felsic intrusions, particularly quartz–feldspar porphyry, act as mechanically competent and chemically reactive cores that localize damage zones and dense quartz–carbonate ± tourmaline vein networks along their margins near the brittle–ductile transition. Where these intrusive margins coincide with NE-trending shear planes and high-density intersection lineations, fracture connectivity and fluid focusing are maximized, giving rise to continuous, steeply plunging ore shoots. These structurally driven criteria can be tested and refined through future near-mine mapping and stepout drilling along the Missira–Kiesta–Nouma corridor by explicitly evaluating whether new anomalies coincide with shear bends, albitized intrusive margins, and the predicted steep SE-plunging intersection lineations.

These insights yield transferable exploration criteria across Sabodala–Massawa and analogous Mako Belt corridors: (i) prioritize bends and stepovers within master corridors; (ii) target felsic intrusive margins showing alteration-induced embrittlement (albitization, silicification) and elevated fracture density; (iii) use intersection lineations to predict shoot plunge; and (iv) follow alteration vectors from outer sericite–carbonate halos toward inner silica- and sulfide-rich assemblages. Depth targeting should emphasize horizons near the BDT where permeability cycling is maximized.

Finally, we note current limitations—absence of direct geochronology on vein formation and quantitative 3D modeling of the fracture network—and identify future work in isotopic dating of vein minerals and geomechanical simulations to refine the timing of fluid events and to quantify permeability architecture.

Declaration by Authors

Acknowledgement: None
Source of Funding: None
Conflict of Interest: No conflicts of interest declared.

REFERENCES

1. Groves DI, Goldfarb RJ, Robert F, Hart CJ. Gold deposits in metamorphic belts: Overview of current understanding, outstanding problems, future research, and exploration significance. Econ. Geol. 2003 ; 98 :1-29.
2. Bessoles B. Géologie de l'Afrique. Vol. 1 : Le Craton Ouest Africain. Orléans (France) : Bureau de Recherches Géologiques et Minières (BRGM) ; 1977. 402 p.
3. Milési JP, Ledru P, Feybesse JL, Dommanget A, Marcoux E. Early Proterozoic ore deposits and tectonics of the Birimian orogenic belt, West Africa. Precambrian Res. 1992; 58:305-344.
4. Baratoux L, Metelka V, Naba S, et al. Juvenile Paleoproterozoic crust evolution during the Eburnean orogeny (~2.2–2.0 Ga), western Burkina Faso. Precambrian Res. 2011; 191:18-45.
5. Jessell MW, Begg GC, Miller MS. The geophysical signatures of the West African Craton. Precambrian Res. 2016; 274:3-24.
6. Markwitz V, Hein KA, Jessell MW, Miller J. Metallogenic portfolio of the West Africa craton. Ore Geol. Rev. 2016; 78:558-563.
7. Goldfarb RJ, André-Mayer AS, Jowitt SM, Mudd GM. West Africa: The world's premier Paleoproterozoic gold province. Econ. Geol. 2017; 112:123-143.
8. Le Pape F, Jones AG, Jessell MW, et al. The nature of the southern West African craton lithosphere inferred from its electrical resistivity. Precambrian Res. 2021; 358:106190.
9. Baratoux L, Jessell MW, Kouamelan AN. The West African Craton. In: Hamimi Z,

Charaf M, Errami E, Fowler AR, Fello N, Masrouhi A, Leprêtre R, editors. The Geology of North Africa. Cham (Switzerland): Springer; 2024. p.47-68.
10. Sylvester PJ, Attoh K. Lithostratigraphy and composition of 2.1 Ga greenstone belts of the West African Craton and their bearing on crustal evolution and the Archean–Proterozoic boundary. J. Geol. 1992 ; 100 :377-393.
11. Feybesse JL, Billa M, Guerrot C, et al. The Paleoproterozoic Ghanaian province: Geodynamic model and ore controls, including regional stress modeling. Precambrian Res. 2006 ; 149 :149-196.
12. Parra-Avila LA, Belousova E, Fiorentini ML, et al. Crustal evolution of the Paleoproterozoic Birimian terranes of the Baoulé–Mossi domain, southern West African Craton: U–Pb and Hf-isotope studies of detrital zircons. Precambrian Res. 2016; 274:25-60.
13. Grenholm M. The global tectonic context of the ca. 2.27–1.96 Ga Birimian orogen—Insights from comparative studies, with implications for supercontinent cycles. Earth-Sci. Rev. 2019; 193:260-298.
14. Ledru P, Pons J, Milési JP, et al. Transcurrent tectonics and polycyclic evolution in the Lower Proterozoic of Senegal–Mali. Precambrian Res. 1991; 50:337-354.
15. Begg GC, Griffin WL, Natapov LM, et al. The lithospheric architecture of Africa: Seismic tomography, mantle petrology, and tectonic evolution. Geosphere. 2009; 5:23-50.
16. Feybesse JL, Milési JP. The Archaean/Proterozoic contact zone in West Africa: A mountain belt of décollement thrusting and folding on a continental margin related to 2.1 Ga convergence of Archaean cratons? Precambrian Res. 1994; 69:199-227.
17. Abouchami W, Boher M, Michard A, Albarède F. A major 2.1 Ga event of mafic magmatism in West Africa: An early stage of crustal accretion. J. Geophys. Res. 1990; 95:17605-17629.
18. Jessell M, Liégeois JP. 100 years of research on the West African Craton. J. Afr. Earth Sci. 2015; 112:377-381.
19. Hirdes W, Davis DW. U–Pb geochronology of Paleoproterozoic rocks in the southern part of the Kedougou–Kenieba Inlier, Senegal, West Africa: Evidence for diachronous accretionary development of the Eburnean province. Precambrian Res. 2002 ; 118 :83-99.
20. Parra-Avila LA, Baratoux L, Eglinger A, et al. The Eburnean magmatic evolution across the Baoulé–Mossi domain: Geodynamic implications for the West African Craton. Precambrian Res. 2019; 332:105392.
21. Groves DI, Goldfarb RJ, Gebre-Mariam M, et al. Orogenic gold deposits: A proposed classification in the context of their crustal distribution and relationship to other gold deposit types. Ore Geol. Rev. 1998; 13:7-27.
22. Guéye M, Ngom PM, Diène M, et al. Intrusive rocks and tectono-metamorphic evolution of the Mako Paleoproterozoic belt (Eastern Senegal, West Africa). J. Afr. Earth Sci. 2008; 50:88-110.
23. Guéye M, van den Kerkhof AM, Hein UF, et al. Structural control, fluid inclusions and cathodoluminescence studies of Birimian gold-bearing quartz vein systems in the Paleoproterozoic Mako belt, southeastern Senegal. S. Afr. J. Geol. 2013; 116:199-218.
24. Guéye M, Siegesmund S, Wemmer K, et al. new evidence for an early Birimian evolution in the West African Craton: An example from the Kédougou–Kéniéba Inlier, SE Senegal. S. Afr. J. Geol. 2007; 110:511-534.
25. Sibson RH. Conditions for fault-valve behaviour. Geol. Soc. Lond. Spec. Publ. 1990; 54:15-28.
26. Cox SF. Faulting processes at high fluid pressures: An example of fault valve behavior from the Wattle Gully Fault, Victoria, Australia. J. Geophys. Res. Solid Earth. 1995; 100:12841-12859.
27. Béziat D, Dubois M, Debat P, et al. Gold metallogeny in the Birimian craton of Burkina Faso (West Africa). J. Afr. Earth Sci. 2008; 50:215-233.
28. Bierlein FP, Northover HJ, Groves DI, et al. Controls on mineralisation in the Sierra Foothills gold province, central California, USA: A GIS-based reconnaissance prospectivity analysis. Aust. J. Earth Sci. 2008; 55:61-78.
29. Groves DI, Santosh M, Goldfarb RJ, et al. Structural geometry of orogenic gold deposits: Implications for exploration of world-class and giant deposits. Geosci. Front. 2018; 9:1163-1177.

30. Witt WK, Hagemann SG, Fisher CF. Diverse examples of sodic and sodic–calcic alteration in greenstone rocks and intrusions of the Kalgoorlie–Kurnalpi Rift, Yilgarn Craton: Significance for gold mineralisation. Aust. J. Earth Sci. 2025; In press:1-31.
31. Teranga Gold Corporation. Sabodala–Massawa Project, Senegal: Pre-Feasibility Study, NI 43-101 Technical Report. Toronto (ON, Canada): Teranga Gold Corporation; 2020. Effective date: 31 Dec 2019.
32. Goldfarb RJ, Pitcairn I. Orogenic gold: Is a genetic association with magmatism realistic? Miner. Deposita. 2023 ; 58 :5-35.
33. Tavares Nassif M, Monecke T, Reynolds TJ, et al. Formation of orogenic gold deposits by progressive movement of a fault-fracture mesh through the upper crustal brittle–ductile transition zone. Sci. Rep. 2022; 12:17379.
34. Allibone A. Timing and structural controls on gold mineralization at the Bogoso gold mine, Ghana, West Africa. Econ. Geol. 2002; 97:949-969.
35. Allibone, A., McCuaig, T. C., Harris, D., Etheridge, M., Munroe, S., & Byrne, D. (2002). Structural Controls on Gold Mineralization at the Ashanti Gold Deposit, Obuasi, Ghana. In R. J. Goldfarb, & R. L. Nielsen (Eds.), Special Publication 9: Integrated Methods for Discovery: Global Exploration in the Twenty-First Century (pp. 65-93). Society of Economic Geologists. https://doi.org/10.5382/SP.09.04
36. Allibone A, Hayden P, Cameron G, Duku F. Paleoproterozoic gold deposits hosted by albite- and carbonate-altered tonalite in the Chirano district, Ghana, West Africa. Econ. Geol. 2004; 99:479-497.

How to cite this article: Ibrahima Dia, Ibrahima Sow. Lithostructural controls on orogenic gold at the Kiesta C deposit, Sabodala-Massawa District, Senegal. *International Journal of Research and Review*. 2025; 12(12): 793-814. DOI: *https://doi.org/10.52403/ijrr.20251281*

******